The Astrophysical Journal, 869:20 (7pp), 2018 December 10 https://doi.org/10.3847/1538-4357/aae6c7

A High Space Density of L^* Active Galactic Nuclei at $z \sim 4$ in the COSMOS Field

K. Boutsia[1], A. Grazian[2], E. Giallongo[2], F. Fiore[3], and F. Civano[4]
[1] Carnegie Observatories, Las Campanas Observatory, Casilla 601, La Serena, Chile; kboutsia@carnegiescience.edu
[2] INAF-Osservatorio Astronomico di Roma, via Frascati 33, I-00078, Monte Porzio Catone, Italy
[3] INAF-Osservatorio Astronomico di Trieste, via G.B. Tiepolo 11, I-34131, Trieste, Italy
[4] Harvard-Smithsonian Center for Astrophysics (CfA), 60 Garden Street, Cambridge, MA 02138, USA
Received 2018 August 2; revised 2018 September 23; accepted 2018 October 6; published 2018 December 6

Abstract

Identifying the source population of ionizing radiation, responsible for the reionization of the universe, is currently a hotly debated subject with conflicting results. Studies of faint, high-redshift star-forming galaxies, in most cases, fail to detect enough escaping ionizing radiation to sustain the process. Recently, the capacity of bright quasi-stellar objects to ionize their surrounding medium has been confirmed also for faint active galactic nuclei (AGNs), which were found to display an escaping fraction of ∼74% at $z \sim 4$. Such levels of escaping radiation could sustain the required UV background, given the number density of faint AGNs is adequate. Thus, it is mandatory to accurately measure the luminosity function of faint AGNs ($L \sim L^*$) in the same redshift range. For this reason we have conducted a spectroscopic survey, using the wide field spectrograph IMACS at the 6.5 m Baade Telescope, to determine the nature of our sample of faint AGN candidates in the COSMOS field. This sample was assembled using photometric redshifts, color, and X-ray information. We ended up with 16 spectroscopically confirmed AGNs at $3.6 < z < 4.2$ down to a magnitude of $i_{AB} = 23.0$ for an area of 1.73 deg^2. This leads to an AGN space density of $\sim 1.6 \times 10^{-6}$ Mpc^{-3} (corrected) at $z \sim 4$ for an absolute magnitude of $M_{1450} = -23.5$. This is higher than previous measurements and seems to indicate that AGNs could make a substantial contribution to the ionizing background at $z \sim 4$. Assuming that AGN physical parameters remain unchanged at higher redshifts and fainter luminosities, these sources could be regarded as the main drivers of cosmic reionization.

Key words: cosmology: observations – galaxies: active – surveys – quasars: general

1. Introduction

The reionization of the universe is the process where neutral hydrogen (H I) becomes ionized and determines the transition from an opaque state to the transparent intergalactic medium (IGM) we observe today. Although the duration of this phase seems to be well established (Fan et al. 2006; Becker et al. 2015; Planck Collaboration et al. 2018), the source population causing this effect is still elusive. The debate is still ongoing as to whether the main contributors are faint, high-redshift, star-forming galaxies (SFGs) or active galactic nuclei (AGNs). For both populations there are critical issues. The assumption for the galaxies being main contributors is that all faint SFGs should present an escape fraction of ionizing radiation f_{esc} of 10%–20% (Finkelstein et al. 2015; Bouwens et al. 2016), which has not been observed so far, apart from in a handful of sources (Shapley et al. 2016; Vanzella et al. 2016; Bian et al. 2017; Steidel et al. 2018). Recent results (Fletcher et al. 2018; Jones et al. 2018; Naidu et al. 2018; Tanvir et al. 2018) do not provide clear evidence, but indicate that it is difficult for the global SFG population to reach the 10%–20% level of escape fraction required to drive the reionization process. The main objection against AGNs being the main contributors is that the number of bright quasars at $z > 4$ is not enough (Fan et al. 2006; Cowie et al. 2009; Haardt & Madau 2012) and the number of faint AGNs at high redshifts is still not well constrained. Based on X-ray samples, at low luminosities in this redshift range, the space density of obscured AGNs is at least two times higher than the unobscured population (Marchesi et al. 2016b), indicating that optically selected luminosity functions (LFs) could only be a lower limit.

In order to answer the question of whether faint AGNs can contribute to the ionizing ultraviolet background (UVB), three aspects need to be quantified: (i) the exact level of the UVB; (ii) the fraction of ionizing radiation escaping these sources (f_{esc}); and (iii) the faint slope of the AGN LF.

Observations of the ionizing UVB intensity in the redshift range $2 < z < 5$ and the global emissivity of ionizing photons indicate a relatively flat hydrogen photoionization rate (Becker & Bolton 2013), but not spatially uniform (Bosman et al. 2018). Such large opacity fluctuations cannot be easily explained by low clustering populations like ultra-faint galaxies and could require the existence of rare bright sources at high redshift (Becker et al. 2015, 2018; Chardin et al. 2015, 2017). As models start including larger AGN contributions, predicted temperatures are in agreement with observational constraints at $z \sim 4$–6 (Keating et al. 2018) (but see Puchwein et al. 2018 for a different interpretation).

Thus, a sizable population of faint ($L \sim L^*$) AGNs could contribute significantly to the UVB, as long as enough H I ionizing photons manage to escape the host galaxy (Madau & Haardt 2015; Khaire et al. 2016). In this respect, a recent study by Grazian et al. (2018), using deep optical/UV spectroscopy, found that faint AGNs ($L \sim L^*$) at $3.6 < z < 4.2$ present high escape fractions of ionizing radiation, with a mean value of 74%. This is in agreement with similar studies of bright quasars ($M_{1450} \leqslant -26$) at the same redshift range (Cristiani et al. 2016), and there is no indication of dependence on absolute luminosities. This means that, if such results are extrapolated to higher redshift ($5 < z < 7$), the AGN contribution to the cosmic reionization process can become significant. At this point, knowledge of the exact number of faint AGNs at

redshifts $z > 4$ becomes crucial in accurately determining the level of this contribution.

Currently the consensus is that the LF for bright AGNs is well constrained, showing a peak at $z \sim 3$ and then rapidly declining (Bongiorno et al. 2007; Croom et al. 2009). However, for $z > 3$ the debate is still open, with various studies presenting contradicting results. Works presented by Ikeda et al. (2011) and Glikman et al. (2011) suggest that the number of faint AGNs at $z > 3$ is higher than expected, producing a steeper slope at the faint end of the LF. But although the faint-end slopes are similar, the normalization factor Φ^* derived by Glikman et al. (2011) is three times higher than that calculated by Ikeda et al. (2011) and subsequently reproduced by other studies (i.e Masters et al. 2012; Akiyama et al. 2018). These latter studies report a strong decline in AGN numbers going from $z = 3$ to $z = 4$. In other words, there is still wide disagreement on the actual shape and normalization of the LF at $z \sim 4$.

Work by Giallongo et al. (2015), including photometric and spectroscopic redshifts of X-ray-selected AGN candidates in the CANDELS GOODS-South region, has shown that at $z > 4$ the probed AGN population could produce the necessary ionization rate to keep the IGM highly ionized (Madau & Haardt 2015). This result is still controversial, with recent works claiming the opposite (i.e., D'Aloisio et al. 2017; Ricci et al. 2017; Akiyama et al. 2018; Hassan et al. 2018; Parsa et al. 2018). In fact, so far, the optical LFs at this redshift range and luminosities are based on a handful of spectroscopically confirmed sources (e.g., eight for Ikeda et al. 2011 and five for Giallongo et al. 2015). Since the bulk of ionizing photons come from AGNs close to L^*, it is mandatory to measure their LF at $z > 4$ in this luminosity range. For this reason, we started a pilot study in the COSMOS field, ideal for this kind of analysis thanks to its multi-wavelength catalog, X-ray, and radio coverage, which allows us to robustly select our AGN candidates. Here we present the bright part of our spectroscopically confirmed sample of intermediate-/low-luminosity AGNs, reaching an absolute magnitude of $M_{1450} = -23$ and discuss a robust determination of the space density at $z \sim 4$.

Throughout the paper we adopt the Λ cold dark matter (ΛCMD) concordance cosmological model ($H_0 = 70$ km s^{-1} Mpc^{-1}, $\Omega_M = 0.3$, and $\Omega_\Lambda = 0.7$). All magnitudes are in the AB system.

2. AGN Candidate Selection

The selection of our sample is based on: (i) photometric redshifts, (ii) color–color selection, and (iii) X-ray emission.

We use the photometric catalog and redshifts presented by Ilbert et al. (2009). This is a 30-band catalog, spanning from NUV photometry to IRAC data, with calculated $z_{\rm phot}$ in a region covering 1.73 deg^2 in COSMOS. The reported $z_{\rm phot}$ dispersion is $\sigma_{(\Delta z)/(z_s+1)} = 0.007$ at $i_{AB} < 22.5$ and increases to $\sigma_{(\Delta z)/(z_s+1)} = 0.012$ at $i_{AB} < 24$. As discussed in Ilbert et al. (2009), their $z_{\rm phot}$ determination is mostly based on galaxy templates. However, as showed by Giallongo et al. (2015), for $z > 4$ the accuracy on the photometric redshift estimate is weakly dependent on the adopted spectral libraries but it is mainly driven by the Lyman break feature at rest frame wavelength (912 Å). To take into account possible larger errors on photometric redshifts for the AGN population, we extended the redshift interval. Thus, we obtained a list of 42 candidates that have a photometric redshift estimate in the interval $3.0 \leqslant z_{\rm phot} \leqslant 5.0$ and a magnitude $i_{AB} < 23.0$.

To increase our selection efficiency and mitigate shortcomings of the $z_{\rm phot}$ technique, we include a color criterion. Since we have a wide number of bands available, initially we explored various combinations of color–color selections, i.e., (B_J–V_J) versus (r–i), (B_J–r) versus (r–i), (g–r) versus (r–i), (u_*–B_J) versus (r–i), and (u_*–g) versus (r–i). Cross-correlating those candidates with known AGNs from the literature, and after exploratory spectroscopy with LDSS-3,[5] for this pilot study we narrowed down our selection to the most promising criterion, i.e., (B_J–V_J) versus (r–i). In the (B_J–V_J) versus (r–i) color–color diagram we consider as high-redshift AGN candidates the sources found in the locus delimited by:

$$(B_J\text{–}V_J) > 1.3$$
and
$$(\text{r–i}) \leqslant 0.60 \times (B_J\text{–}V_J) - 0.30.$$

With this criterion we obtained 23 candidates down to $i_{AB} = 23.0$, summarized in Table 1. We decided not to put any constraints on the morphology, since the population of low-luminosity AGNs ($M_{1450} \sim -23$) includes Seyferts, where the host galaxy could be visible.

There is a relatively small overlap between the candidates selected by the various methods. More specifically, only 7% of the candidates selected by photometric redshifts are also included in the color-selected sample (three out of 42 objects), which is useful to increase our completeness. This is a clear advantage with respect to the works of Glikman et al. (2011) and Ikeda et al. (2011) which only used four bands for their selections.

The final criterion for the creation of our sample was X-ray emission. In practice, we selected 38 sources detected in X-rays by deep *Chandra* observations in the COSMOS field (Civano et al. 2016) with $z_{\rm phot} \geqslant 3$ and a limiting magnitude $i_{AB} < 23$. These photometric redshifts were provided by Marchesi et al. (2016a) based on AGNs, galaxies, or hybrid templates, as described in Salvato et al. (2011). This sample consists both of type-1 and type-2 AGNs, and represents an unbiased census of the faint AGN population at this redshift. Only eight of the sources selected with the first two criteria present also emission in X-rays, while six candidates have been selected both by X-ray and color criteria.

Our final sample consists of 92 AGN candidates with magnitudes $i_{AB} < 23$, selected by at least one of the methods mentioned above. Thanks to extensive spectroscopic campaigns carried out in the COSMOS field (e.g., Brusa et al. 2009; Ikeda et al. 2011; Civano et al. 2012; Marchesi et al. 2016a; Hasinger et al. 2018), 22 of our 92 candidates have secure spectroscopic redshifts. To establish the nature of the remaining 70 sources (five of which have uncertain spectroscopic redshifts), we started an exploratory spectroscopic campaign at the Magellan Telescopes.

3. Spectroscopic Follow-up

We were awarded 2.5 nights with the wide-field Inamori–Magellan Areal Camera and Spectrograph (IMACS, Dressler et al. 2011) on the 6.5 m Magellan–Baade telescope at Las Campanas Observatory to obtain spectra for our AGN candidates. We observed a total of five multi-slit masks with the IMACS f/2 camera (27′ diameter field of view) with total

[5] http://www.lco.cl/telescopes-information/magellan/instruments/ldss-3

Table 1
Color–Color Candidates

ID	R.A.	Decl.	i_{AB}	z_{phot}	z_{spec}	(B_J-V_J)	(r–i)	X-ray
658294[a]	149.467350	1.855592	21.056	−1.000	4.174	1.40	0.25	no
1856470[a]	150.475680	2.798362	21.282	0.000	4.110	1.42	0.32	yes
1581239	150.746170	2.674495	21.556	0.293	−1.000	1.77	0.48	no
507779	150.485630	1.871927	22.034	0.605	4.450	4.94	0.55	yes
38736[a]	150.732540	1.516127	22.088	−1.000	4.183	1.69	0.64	no
1226535	150.100980	2.419435	22.325	0.480	4.637	1.68	0.43	yes
422327	149.701500	1.638375	22.409	0.343	3.201	1.54	0.14	no
664641[a]	149.533720	1.809260	22.436	0.338	3.986	1.69	0.30	no
1163086[a]	150.703770	2.370019	22.444	−1.000	3.748	1.44	0.25	yes
330806[a]	150.107380	1.759201	22.555	3.848	4.140	1.48	0.30	yes
344777	150.188180	1.664540	22.634	0.392	−1.000	1.89	−0.44	no
1450499	150.115830	2.563627	22.685	0.280	3.355	1.94	0.63	no
1687778	150.006940	2.779943	22.715	0.437	−1.000	1.96	0.44	no
96886	150.289380	1.559480	22.765	3.860	−1.000	1.77	0.27	no
1573716	150.729200	2.739130	22.783	0.376	−1.000	1.35	0.48	no
346317	150.205950	1.654837	22.800	0.352	−1.000	1.450	−0.21	no
1257518	150.025190	2.371214	22.810	0.241	−1.000	1.60	0.34	no
1322738	149.444050	2.424602	22.839	0.428	−1.000	1.92	0.71	no
1663056	150.185000	2.779340	22.862	3.658	−1.000	2.29	0.52	no
1719143	149.755390	2.738555	22.873	−1.000	3.535	1.76	0.23	yes
125420	150.222680	1.510574	22.898	0.181	−1.000	1.83	0.53	no
867305	149.446230	2.115336	22.950	0.651	−1.000	2.11	0.71	no
612661	149.838500	1.829048	23.011	4.229	4.351	1.93	0.60	no

Note.
[a] Used for the LF.

exposure times ranging from 3 to 6 hr, during dark time in 2018 February and March. The width of the slits was 1.″0 and the detector was used without binning (0.″2/pixel in the spatial direction).

For the three 6 hr masks we used the 300 line mm^{-1} red-blazed grism (300_26.7) with spectral sampling of 1.25 Å $pixel^{-1}$, while for the two 3 hr masks we used the 200 line mm^{-1} grism that has a slightly lower resolution, sampling 2.04 Å $pixel^{-1}$. It is worth noting that the space density of our AGN candidates is such that only around three objects typically fall in an IMACS field of view at this magnitude limit.

We observed a total of 16 AGN candidates with magnitudes ranging from $i_{AB} = 20$ to 23.0, and for 14 of them we obtained robust redshift determination at $z > 3$, resulting in an efficiency of ∼88%, and two uncertain redshifts at $z > 3$. Out of the subsample with secure redshifts, we found six AGNs in the redshift range $3.6 \leqslant z_{spec} \leqslant 4.2$, and eight AGNs with a measured redshift of either $3.1 < z_{spec} < 3.6$ or $4.2 < z_{spec} < 4.7$. The masks were completed with less reliable AGN candidates at $z \sim 4$ obtained by relaxing the criteria mentioned above and exploring different color selections with respect to the $(B_J–V_J)$ versus (r–i) one. We also added, as fillers, fainter candidates, $i_{AB} \leqslant 24.0$, in order to explore the fainter regime of the AGN LF.

After the spectroscopic campaign, 36 sources of the parent sample of 92 candidates had secure spectroscopic redshifts. In addition, seven sources had uncertain spectroscopic classification, either because of low signal-to-noise ratio or because only one line was visible. This left 49 candidates with no redshift information. Figure 1 shows the spectra of the six AGNs with $3.6 \leqslant z_{spec} \leqslant 4.2$ and $i_{AB} \leqslant 23.0$ discovered during our spectroscopic campaign with IMACS and LDSS-3. Most sources show characteristic AGN lines like Si IV and C IV. The two sources that do not show Si IV and C IV have been included for other

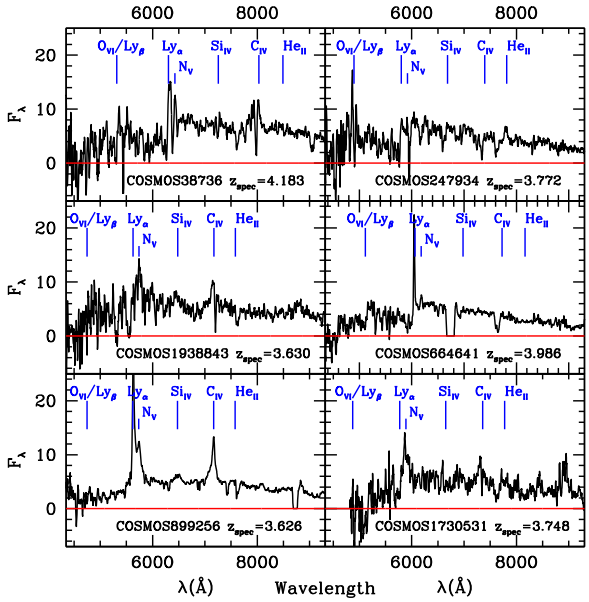

Figure 1. Spectra of the six AGNs with $3.6 \leqslant z \leqslant 4.2$ and $i_{AB} \leqslant 23.0$ discovered during our spectroscopic campaign with IMACS and LDSS-3. The red line corresponds to zero flux F_λ, in arbitrary units.

strong high-ionization lines that are also characteristic of AGNs. More specifically, COSMOS664641 has strong O VI and N V lines, while the C IV line falls in a region of telluric absorption and this could be the reason it is not observed. In the case of COSMOS247934 we also detect strong O VI/Lyβ, as well as He II lines, and it is relatively bright with $M_{1450} \sim -23.2$. The fact that these sources lack X-ray emission does not preclude their AGN nature, since there is a number of examples of AGNs not detected by deep X-ray surveys (Steidel et al. 2002).

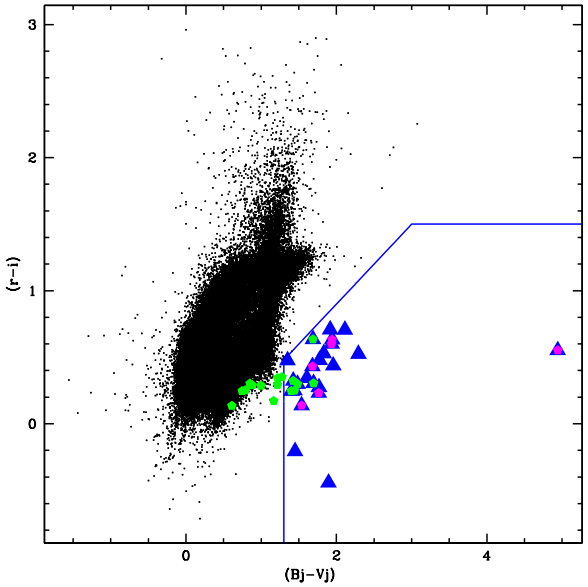

Figure 2. Color–color diagram. Blue triangles show candidates selected by color. Pentagons show candidates selected by photometric redshifts or X-ray emission and confirmed by spectroscopy as AGNs. Green pentagons correspond to AGNs at $3.6 < z_{spec} < 4.2$ and magenta pentagons show confirmed AGNs that have either $z_{spec} < 3.6$ or $z_{spec} > 4.2$. Notice that half of the confirmed AGNs are found outside the color selection locus and that half of the color selected candidates still need to be observed.

Moreover, their luminosities ($M_{1450} \leqslant -23.5$) are another indication of their nuclear activity. In the subsequent analysis we only consider sources with secure spectroscopic redshifts either from our campaign or from the literature.

The distribution of our candidates in the color–color space can be seen in Figure 2. Here we plot the entire color-selected sample and indicate which sources were confirmed as AGNs, in the redshift range of interest, either after our spectroscopic campaign or from the literature. We also indicate sources that lie in the color locus but their spectroscopic redshifts are either $z_{\rm spec} < 3.6$ or $z_{\rm spec} > 4.2$. A detailed presentation of the full spectroscopic sample and a comprehensive description of the different color criteria are not the main aims of the present paper and will be discussed in a future work.

4. Space Density Determination

The advantage of doing this study in the COSMOS field is that it already contains extensive spectroscopic follow-up and extensive multi-wavelength data from radio to X-rays. Thus, combining the confirmed candidates presented above, with known AGNs from the literature, we obtain a sample of 16 spectroscopically confirmed AGNs with $3.6 < z < 4.2$ and $i_{AB} < 23$, presented in Table 2, along with the relative r_{AB} for each source. The i_{AB} magnitudes are from *HST* F814W band, while the r_{AB} magnitudes are from the Subaru telescope and they are described in Ilbert et al. (2009).

The absolute magnitude at 1450 Å rest frame (M_{1450}) for each source has been derived from the r_{AB} magnitude applying a K-correction according to the following formula:

$$M_{1450} = r_{AB} - 2.5\log(1 + z_{\rm spec}) + K_{\rm corr} \quad (1)$$

where

$$K_{\rm corr} = 2.5\alpha_\nu \log_{10}(\lambda_{\rm obs}/(1 + z_{\rm spec})/\lambda_{\rm rest}). \quad (2)$$

The AGN intrinsic slope α_ν is fixed to -0.7, while $\lambda_{\rm obs} = 6284$ Å is the central wavelength of the r_{AB} filter and $\lambda_{\rm rest} = 1450$ Å. The reason we chose the r_{AB} band is because it is not affected by strong quasar emission lines, like C IV that falls in the i_{AB} band for this redshift range. The K-correction is redshift dependent and ranges from 0.05 mag at $z = 3.6$ to 0.14 mag at $z = 4.2$. To check the robustness of our absolute magnitude determination, we have used various methods to calculate it (using the i and r band, with and without K-correction). The point at $M_{1450} = -24.5$ remains basically unaltered, and we only see small changes in it at $M_{1450} = -23.5$, with the current determination resulting in the faintest absolute magnitudes, thus being the most conservative.

We find four sources for $-25 < M_{1450} < -24$ and 9 for $-24 < M_{1450} < -23$. Based on these numbers, we calculate the space density of AGNs at this redshift range in the two magnitude bins. This space density, summarized in Table 3, has been derived by dividing the actual number of the spectroscopically confirmed AGNs with the comoving volume between $3.6 \leqslant z \leqslant 4.2$, without any correction for incompleteness. Thus it represents a robust lower limit to the real space density of $z \sim 4$ AGNs. As can be seen in Figure 3, without any corrections (blue filled squares), our measurements agree well with the Glikman et al. (2011) analysis and put more stringent constraints on the knee of the LF.

Considering completeness and contamination, we can estimate rough corrections. In the color selection, we have six AGNs with $3.6 < z_{\rm spec} < 4.2$ out of 12 AGNs with known $z_{\rm spec}$. Thus, out of the 11 candidates without $z_{\rm spec}$, we expect five or six (∼50%) to have $3.6 < z_{\rm spec} < 4.2$, resulting to 11 or 12 potential AGNs with the (B_J–V_J) versus (r–i) selection. The known AGNs with $3.6 < z_{\rm spec} < 4.2$ and $i_{AB} \leqslant 23.0$ are 16, of which we recover 37.5% with the (B_J–V_J) versus (r–i) criterion (six out of 16). This means that the total number of AGNs expected in COSMOS at $3.6 < z_{\rm spec} < 4.2$ and $i_{AB} < 23.0$ could be $N_{\rm tot} = 11 \times 16/6 = 29.3$ or $N_{\rm tot} = 12 \times 16/6 = 32$. The space density determination using only the 16 AGNs known at $3.6 < z_{\rm spec} < 4.2$, $i_{AB} \leqslant 23.0$ and $-26.0 < M_{1450} < -23.0$ is incomplete by a factor of 0.50–0.55 at least. If we correct for this incompleteness factor, we will go to a level higher than Glikman et al. (2011) (green open squares in Figure 3). Adopting a slightly different color criterion, with $(B_J - V_J) > 1.1$ instead of 1.3 as threshold, the expected total number of AGNs is 34 and the completeness corrections remain at the ∼50% level. This indicates that the green squares (corrected space density) in Figure 3 are quite robust with respect to the details of the adopted color criterion.

In Figure 3 we also present the LFs calculated by Akiyama et al. (2018), Parsa et al. (2018), and Masters et al. (2012) for comparison. The sample created by Akiyama et al. (2018) is limited to g-band dropout (i.e., $3.5 < z < 4.0$) point-like sources, for which they have derived photometric redshifts based on five filters (g, r, i, z, y). The faint-end slope presented in their work is too shallow to be reconciled with our measurements, which correspond to spectroscopically confirmed sources. The LF by Ikeda et al. (2011) is also lower than our space density determination. On the other hand Parsa et al. (2018), after performing an independent photometric redshift estimate of the X-ray-selected sample presented by Giallongo et al. (2015), discarded 10 of the 22 sources that were supposed to lie at $z > 4$. Even though the faint-end slope in Parsa et al. (2018) is steeper

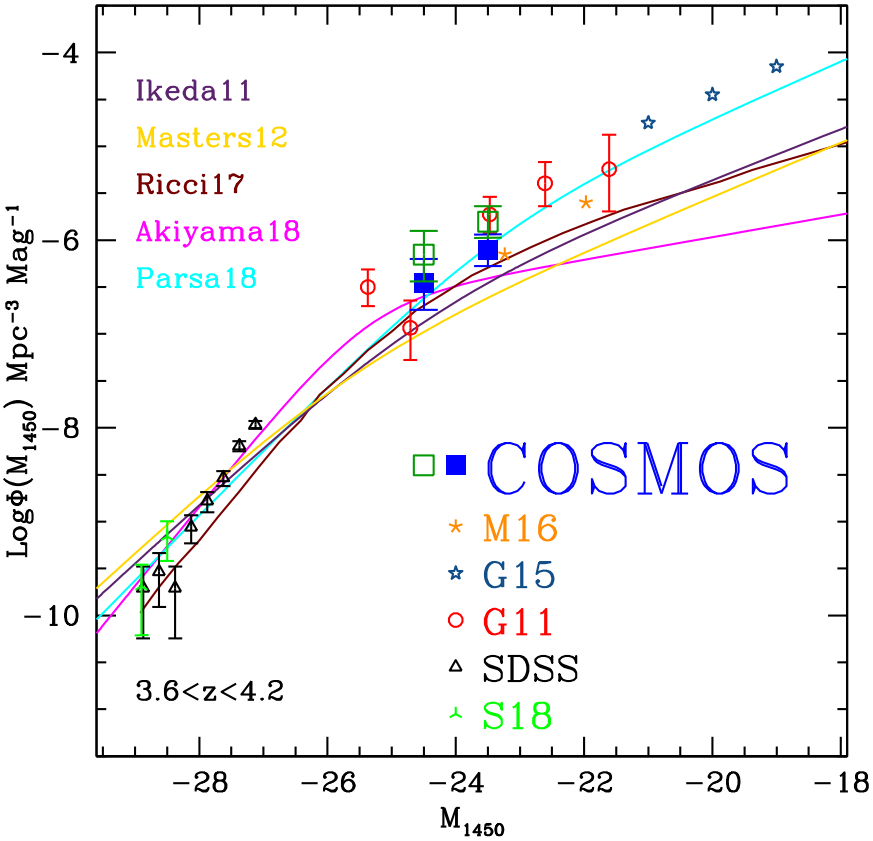

Figure 3. Luminosity function of quasi-stellar objects/AGNs at $z \sim 4$. Black triangles show the bright end determined by the SDSS (Akiyama et al. 2018), green triangles are the points presented by Schindler et al. (2018), red circles show the bins calculated by Glikman et al. (2011), blue stars show the bins by Giallongo et al. (2015), filled blue squares represent the two magnitude bins from this work (no corrections), and the open green squares correspond to the space density derived in this work after applying the corrections discussed in Section 4. Notice that our data actually compensate for the apparent dip present in the work by Glikman et al. (2011). The results by Marchesi et al. (2016b), converted into UV, are presented as orange asterisks. For comparison we also present the LFs derived by Ikeda et al. (2011), Masters et al. (2012), Ricci et al. (2017), Akiyama et al. (2018), and Parsa et al. (2018). All LFs have been evolved to $z = 3.9$ following the density evolution law by Fan et al. (2001).

Table 2
Confirmed AGNs Used for Determining Space Density

ID	R.A.	Decl.	i_{AB}	z_{spec}	r_{AB}	M_{1450}	References
38736	150.732540	1.516127	22.088	4.183	22.897	−23.341	our spectroscopy
247934	150.801300	1.657550	22.334	3.772	22.817	−23.182	our spectroscopy
330806	150.107380	1.759201	22.555	4.140	23.105	−23.110	Ikeda et al. (2011)
658294	149.467350	1.855592	21.056	4.174	21.603	−24.630	Trump et al. (2009)
664641	149.533720	1.809260	22.436	3.986	22.946	−23.182	our spectroscopy
899256	150.782210	2.285049	21.927	3.626	22.363	−23.545	our spectroscopy
1054048[a]	149.879200	2.225839	22.697	3.650	23.200	−22.722	Marchesi et al. (2016a)
1159815	150.638440	2.391350	22.157	3.650	22.539	−23.383	Ikeda et al. (2011)
1163086	150.703770	2.370019	22.444	3.748	22.863	−23.122	Marchesi et al. (2016a)
1208399	150.259540	2.376141	21.424	3.717	21.488	−24.478	Marchesi et al. (2016a)
1224733	150.208990	2.438466	21.147	3.715	21.485	−24.480	Marchesi et al. (2016a)
1273346[a]	149.776910	2.444306	22.779	4.170	23.274	−22.952	Marchesi et al. (2016a)
1730531[a]	149.843220	2.659095	22.900	3.748	23.439	−22.545	our spectroscopy
1856470	150.475680	2.798362	21.282	4.110	21.753	−24.445	Marchesi et al. (2016a)
1938843	149.845860	2.860459	22.160	3.630	22.619	−23.290	our spectroscopy
1971812	149.472870	2.793400	21.887	3.610	22.179	−23.717	Marchesi et al. (2016a)

Note.
[a] Not included in the space density bins because $M_{1450} > -23.0$.

than that found by Glikman et al. (2011), their space density in absolute magnitudes $M_{1450} < -23$ is marginally in agreement with our estimates. We also show the space density derived by Marchesi et al. (2016b), based on X-ray data, after being converted to UV (Ricci et al. 2017). Although these points are higher than most optical LFs, they are slightly lower than our estimate. In Table 3 we present the estimate of the AGN space density Φ, based on our analysis, in the two absolute magnitude bins. Even

Table 3
AGN Space Density ($\langle z \rangle = 3.9$)

M_{1450}	Φ $\mathrm{Mpc^{-3}Mag^{-1}}$	$\sigma_{\Phi}^{\mathrm{up}}$	$\sigma_{\Phi}^{\mathrm{low}}$	N_{AGN}	Φ_{corr}
−24.5	3.509e-07	2.789e-07	1.699e-07	4	7.018e-07
−23.5	7.895e-07	3.616e-07	2.595e-07	9	1.579e-06

excluding the COSMOS247934, which is the least certain among our sources, the uncorrected space density at $M_{1450} = -23.5$ becomes 7.018e-07 $\mathrm{Mpc^{-3}Mag^{-1}}$, which is still higher than all LFs presented in Figure 3, except for Parsa et al. (2018). Considering the space density corrected for incompleteness, the Parsa et al. (2018) LF also turns out to be underestimated.

An important aspect, made clear by our sample, is that selections based on color criteria can be highly incomplete, since out of the 16 spectroscopically confirmed AGNs only six have been selected by color. So far, the majority of studies on the AGN LF at this redshift range is based on color-selected samples and this could be the reason why faint AGN number densities have been underestimated. When a first attempt was made by Giallongo et al. (2015) to create an AGN sample based on non-traditional criteria, a different picture emerged. Given that AGNs, even at faint magnitudes, have a large escape fraction as shown by Grazian et al. (2018), an increase of the estimate of their population can have significant implications on the contribution of AGNs to the H I ionizing background.

5. Discussion and Conclusions

Our estimates of the space density in the range $-24.5 < M_{1450} < -23.5$, shown by filled blue squares in Figure 3, are not corrected for any incompleteness factor, thus they represent firm lower limits, assuming that the density fluctuations due to cosmic variance are not important.

To explore this possibility, we checked how the volume density of AGNs at $z \sim 4$ in COSMOS compares to the average derived from the SDSS survey. In the COSMOS area there is no known quasi-stellar object (QSO) brighter than $i_{AB} = 21.0$ in the redshift interval $3.6 < z < 4.2$. Considering the SDSS DR14 catalog (Pâris et al. 2018) in areas of different sizes, ranging from 10–100 $\mathrm{deg^2}$, centered on the COSMOS field, we find a mean density of $0.59 \pm 0.10\ \mathrm{deg^{-2}}$ compared to the mean SDSS density of $0.61 \pm 0.01\ \mathrm{deg^{-2}}$ (5683 QSOs in 9376 $\mathrm{deg^2}$). This indicates that the COSMOS field is not particularly overdense or underdense at $z \sim 4$. For this reason, the completion of a spectroscopic AGN survey in this field, such as the one presented here, is fundamental to address the role of AGNs in the reionization epoch.

Indeed, the AGN space density derived by our study is a conservative estimate and might increase in the future. As can be seen in Table 1, six confirmed AGNs at $z_{\mathrm{spec}} \geqslant 3$ have $z_{\mathrm{phot}} < 1$ in Ilbert et al. (2009). In two cases, where both the spectroscopic and the photometric redshifts are larger than 3, the z_{phot} tends to systematically underestimate the actual z_{spec}. This is an indication that our selection based on z_{phot} could still be biased against $z \sim 4$ AGNs, and that different z_{phot} recipes could increase the number of AGN candidates selected by photometric redshifts. As an example, Salvato et al. (2011) provided photometric redshifts only for two of our sources in Table 1, i.e., source id = 330806 with $z_{\mathrm{phot}} = 3.949$ and id = 1226535 with $z_{\mathrm{phot}} = 4.545$. Their estimates are in reasonable agreement with the spectroscopic redshifts of these AGNs.

Stevans et al. (2018), in their analysis of the UV LF of a mixed sample including both SFGs and galaxies dominated by AGNs at $z \sim 4$ in the SHELA survey, found a space density of $10^{-6}\ \mathrm{Mpc^{-3}}$ at $M_{1450} = -23.5$. Our measurements in the same redshift and absolute magnitude is $\sim 1.6 \times 10^{-6}\ \mathrm{Mpc^{-3}}$ (corrected), and this is an indication that their LF is dominated by AGNs at $M_{1450} < -23.5$. Based on their discussion, a high AGN space density would mean that AGNs could be largely responsible for the H I ionizing UVB at $z = 4$.

We are confident that on the net of all random and systematic effects, the corrected estimate of the LF presented in this work represents a robust determination of the space density of L^* AGNs at $z \sim 4$. The agreement of our measurement with the Glikman et al. (2011) results favors at $M_{1450} < -23.5$ a steeper slope of the LF for the COSMOS field than that determined by Ikeda et al. (2011), Masters et al. (2012), Ricci et al. (2017), Akiyama et al. (2018), and Parsa et al. (2018).

This study poses an open challenge that should be addressed in the future with major observational effort: to measure with great accuracy the space density of AGNs at $L = L^*$ and $z > 4$. In fact, in a subsequent work, once our spectroscopic sample is complete, we will present the global shape of the LF at $z \sim 4$ and the associated emissivity. This can have deep implications on the extrapolation of the number of QSOs expected at high-z in wide and deep large area surveys, either ground based, e.g. *LSST*, or from space, e.g., e-*Rosita*, *Euclid*, *WFIRST*. An upward revision of the number density of $L = L^*$ AGNs would certainly imply a reconsideration of the expected QSO and AGN numbers at $z > 4$ in these future missions.

We would like to thank the anonymous referee for useful suggestions and constructive comments that helped us improve this paper. This paper includes data gathered with the 6.5 m Magellan Telescopes located at Las Campanas Observatory (LCO), Chile.

ORCID iDs

K. Boutsia https://orcid.org/0000-0003-4432-5037
A. Grazian https://orcid.org/0000-0002-5688-0663
E. Giallongo https://orcid.org/0000-0003-0734-1273

References

Akiyama, M., He, W., Ikeda, H., et al. 2018, PASJ, 70, S34
Becker, G. D., & Bolton, J. S. 2013, MNRAS, 436, 1023
Becker, G. D., Bolton, J. S., Madau, P., et al. 2015, MNRAS, 447, 3402
Becker, G. D., Davies, F. B., Furlanetto, S. R., et al. 2018, ApJ, 863, 92
Bian, F., Fan, X., McGreer, I., Cai, Z., & Jiang, L. 2017, ApJL, 837, L12
Bongiorno, A., Zamorani, G., Gavignaud, I., et al. 2007, A&A, 472, 443
Bosman, S. E. I., Fan, X., Jiang, L., et al. 2018, MNRAS, 479, 1055
Bouwens, R. J., Smit, R., Labbé, I., et al. 2016, ApJ, 831, 176
Brusa, M., Comastri, A., Gilli, R., et al. 2009, ApJ, 693, 8
Chardin, J., Haehnelt, M. G., Aubert, D., & Puchwein, E. 2015, MNRAS, 453, 2943
Chardin, J., Puchwein, E., & Haehnelt, M. G. 2017, MNRAS, 465, 3429
Civano, F., Elvis, M., Brusa, M., et al. 2012, ApJS, 201, 30
Civano, F., Marchesi, S., Comastri, A., et al. 2016, ApJ, 819, 62
Cowie, L. L., Barger, A. J., & Trouille, L. 2009, ApJ, 692, 1476
Cristiani, S., Serrano, L. M., Fontanot, F., Vanzella, E., & Monaco, P. 2016, MNRAS, 462, 2478
Croom, S. M., Richards, G. T., Shanks, T., et al. 2009, MNRAS, 399, 1755
D'Aloisio, A., Upton Sanderbeck, P. R., McQuinn, M., Trac, H., & Shapiro, P. R. 2017, MNRAS, 468, 4691

Dressler, A., Bigelow, B., Hare, T., et al. 2011, PASP, 123, 288
Fan, X., Strauss, M. A., Becker, R. H., et al. 2006, AJ, 132, 117
Fan, X., Strauss, M. A., Schneider, D. P., et al. 2001, AJ, 121, 54
Finkelstein, S. L., Ryan, R. E., Jr., Papovich, C., et al. 2015, ApJ, 810, 71
Fletcher, T. J., Robertson, B. E., Nakajima, K., et al. 2018, arXiv:1806.01741
Giallongo, E., Grazian, A., Fiore, F., et al. 2015, A&A, 578, A83
Glikman, E., Djorgovski, S. G., Stern, D., et al. 2011, ApJL, 728, L26
Grazian, A., Giallongo, E., Boutsia, K., et al. 2018, A&A, 613, A44
Haardt, F., & Madau, P. 2012, ApJ, 746, 125
Hasinger, G., Capak, P., Salvato, M., et al. 2018, ApJ, 858, 77
Hassan, S., Davé, R., Mitra, S., et al. 2018, MNRAS, 473, 227
Ikeda, H., Nagao, T., Matsuoka, K., et al. 2011, ApJL, 728, L25
Ilbert, O., Capak, P., Salvato, M., et al. 2009, ApJ, 690, 1236
Jones, L. H., Barger, A. J., Cowie, L. L., et al. 2018, ApJ, 862, 142
Keating, L. C., Puchwein, E., & Haehnelt, M. G. 2018, MNRAS, 477, 5501
Khaire, V., Srianand, R., Choudhury, T. R., & Gaikwad, P. 2016, MNRAS, 457, 4051
Madau, P., & Haardt, F. 2015, ApJL, 813, L8
Marchesi, S., Civano, F., Elvis, M., et al. 2016a, ApJ, 817, 34
Marchesi, S., Civano, F., Salvato, M., et al. 2016b, ApJ, 827, 150
Masters, D., Capak, P., Salvato, M., et al. 2012, ApJ, 755, 169
Naidu, R. P., Forrest, B., Oesch, P. A., Tran, K.-V. H., & Holden, B. P. 2018, MNRAS, 478, 791
Pâris, I., Petitjean, P., Aubourg, É, et al. 2018, A&A, 613, A51
Parsa, S., Dunlop, J. S., & McLure, R. J. 2018, MNRAS, 474, 2904
Planck Collaboration, Akrami, Y., Arroja, F., et al. 2018, arXiv:1807.06205
Puchwein, E., Haardt, F., Haehnelt, M. G., & Madau, P. 2018, arXiv:1801.04931
Ricci, F., Marchesi, S., Shankar, F., La Franca, F., & Civano, F. 2017, MNRAS, 465, 1915
Salvato, M., Ilbert, O., Hasinger, G., et al. 2011, ApJ, 742, 61
Schindler, J.-T., Fan, X., McGreer, I. D., et al. 2018, ApJ, 863, 144
Shapley, A. E., Steidel, C. C., Strom, A. L., et al. 2016, ApJL, 826, L24
Steidel, C. C., Bogosavlevic, M., Shapley, A. E., et al. 2018, arXiv:1805.06071
Steidel, C. C., Hunt, M. P., Shapley, A. E., et al. 2002, ApJ, 576, 653
Stevans, M. L., Finkelstein, S. L., Wold, I., et al. 2018, ApJ, 863, 63
Tanvir, N. R., Fynbo, J. P. U., de Ugarte Postigo, A., et al. 2018, arXiv:1805.07318
Trump, J. R., Impey, C. D., Elvis, M., et al. 2009, ApJ, 696, 1195
Vanzella, E., de Barros, S., Vasei, K., et al. 2016, ApJ, 825, 41